Modifying the thermal and mechanical properties of poly(lactic acid) by adding lithium trifluoromethanesulfonate

Shota Tomie[1)], Naoya Tsugawa[1,2)], and Masayuki Yamaguchi[1)*]

1) School of Materials Science, Japan Advanced Institute of Science and Technology
1-1 Asahidai, Nomi, Ishikawa 923-1292 JAPAN

2) TOSOH Analysis and Research Center Co.,
1-8 Kasumi, Yokkaichi, Mie 510-8540 JAPAN

*Corresponding author. E-mail address: m_yama@jaist.ac.jp (Masayuki Yamaguchi)
Phone: +81-761-51-1621
Fax: +81-761-51-1149

ABSTRACT

The effect of the addition of lithium trifluoromethanesulfonate ($LiCF_3SO_3$) on the linear viscoelastic properties, crystallization behavior, and mechanical properties of poly(lactic acid) (PLA) was studied. The glass transition temperature (T_g) was enhanced by adding $LiCF_3SO_3$, without any loss of transparency of the PLA. This was attributed to the ion-dipole interaction between the lithium cation and oxygen atom in the PLA carbonyl group. The interaction weakened at higher temperature. Consequently, the rheological terminal region was clearly detected, which suggested that the system possessed good melt-processability. The Young's modulus and yield stress at room temperature were also enhanced by the addition of $LiCF_3SO_3$, although the toughness was reduced due to the brittle failure. Finally, the presence of $LiCF_3SO_3$ retarded the crystallization of PLA, because the segmental motion of the PLA chains was reduced.

Keywords; Poly(lactic acid); Rheology; Crystallization; Glass transition temperature

Introduction

Poly(lactic acid) (PLA) is a well-known biomass-based plastic. It has various attractive properties, such as carbon neutrality, biocompatibility, biodegradability, optical transparency, and good processability [1-5]. Therefore, PLA and its blends/composites have been studied greatly and used in many applications including packaging and housing of electronic products [6-8]. However, its application is still limited by its poor heat resistance [1-5,9], because the glass transition temperature (T_g) of PLA is around 60 °C. A well-known method for enhancing the heat resistance is to increase the crystallinity [1-5]. PLA containing a large amount of crystals exhibits similar dynamic mechanical properties to isotactic polypropylene in the solid state [10]. Much effort has therefore focused on enhancing the crystallization rate of PLA. The addition of nanofillers was proposed for this purpose [11,12], and is now utilized in industry. Addition of nucleating agents [13-15] and/or plasticizers [16-18] can also enhance the crystallization rate. However, high crystallinity usually results in opaque materials owing to light scattering. There is a strong demand for a new technology to prepare transparent PLA products with good heat resistance.

Increasing the molecular weight and introducing crosslinking points will generally enhance the T_g of polymers [19,20] including PLA [21-23]. However, these techniques also tend to result in PLA losing its good melt-processability, and thus are not recommended. In the case of ionomers that have a carboxylic acid group in the polymer chain, the ion-dipole interaction acts as a crosslink point which enhances the T_g [24-26]. Increasing the temperature leads to this interaction weakening, which in turn leads to thermoplastic properties. This strategy for material design can be used to improve the

heat resistance of PLA. The enhancement of the T_g of poly(methyl methacrylate) (PMMA) by adding a specific lithium salt was reported recently, despite PMMA containing no acidic or hydroxyl groups in its main chain [27]. In this system, segmental motion was reduced by the ion–dipole interaction between the lithium cation and PMMA carboxyl group, at temperatures around the T_g. Furthermore, the interaction decreased at high temperature [27]. Although such interaction is expected in various polar polymers, there have been a couple of reports only on PMMA [28,29]. Moreover, the effect of the ion-dipole interaction on crystallinity has not been clarified yet in our previous reports.

In the current study, we added lithium trifluoromethanesulfonate ($LiCF_3SO_3$) into PLA, i.e., one of the most important polyesters and biomass-based materials, to reduce the segmental motion by exploiting the ion-dipole interaction. The rheological properties in the molten state, crystallization behavior, and tensile properties in the solid state were investigated for the resulting blends. The reduced segmental motion of PLA due to the interaction with the salt affected the viscoelastic properties and thermal properties including the crystallization behavior. Although the $LiCF_3SO_3$ addition loses the cost-performance, these findings must provide basic information pertinent to designing various polar polymers including biomass-based plastics.

Experimental

Materials

Two types of commercially available PLA were used. One was crystalline PLA

(cPLA) containing 1% D-lactide. The other was amorphous PLA (aPLA) containing 12% D-lactide. The number-average molecular weight (M_n) and weight-average molecular weight (M_w), as evaluated by gel permeation chromatography (HLC-8020, Tosoh, Japan) using TSK-GEL GMHXL as a polystyrene standard, were $M_n = 9.8\times10^4$ and $M_w = 1.7\times10^5$ for cPLA and $M_n = 1.0\times10^5$ and $M_w = 1.7\times10^5$ for aPLA. Details of the PLA samples are described in our previous papers [30,31]. $LiCF_3SO_3$ was purchased from Kanto Chemical and was used without further purification.

Sample preparation

Prior to melt-mixing, PLA pellets were dried at 80 °C for 4 h under vacuum. PLA and $LiCF_3SO_3$ were mixed in a molten state using an internal mixer (Labo Plastmill, Toyo Seiki, Japan) for 5 min, with a blade rotation speed of 30 rpm. Mixing was performed at 180 °C for aPLA and at 200 °C for cPLA. The concentrations of $LiCF_3SO_3$ were 0, 5, 10, and 20 wt.%. The obtained mixtures were dried at 160 °C for 4 h under vacuum, and then compressed into flat films 300 μm in thickness by a compression-molding machine at 200 °C under 30 MPa for 90 sec. The resulting films were cooled at 25 °C for 3 min. The films were then used immediately to avoid the effects of moisture, since it is known that the moisture may affect the T_g greatly [32].

Measurements

The temperature dependence of dynamic tensile moduli was measured from 25 °C to 200 °C using a dynamic mechanical analyzer (Rheogel E-4000, UBM, Japan). The

frequency and heating rate were 10 Hz and 2 °C/min, respectively.

The frequency dependence of the oscillatory shear modulus was measured using a cone-and-plate rheometer (AR2000ex, TA Instruments, USA) at various temperatures from 90 °C to 180 °C, under a nitrogen atmosphere.

The thermal properties were evaluated using a differential scanning calorimeter (DSC) (DSC 8500, PerkinElmer). The samples were heated from 25 °C to 190 °C at a heating rate of 10 °C/min, and then cooled from 190 °C to 25 °C at a cooling rate of 2 °C/min. Analyses were carried out on approximately 10-mg samples encapsulated in aluminum pans.

Infrared spectra were collected using a Fourier-transform infrared (FT-IR) analyzer (Spectrum 100, PerkinElmer, USA) at room temperature. The measurements were performed in the attenuated total reflection (ATR) mode using KRS-5 as an ATR crystal.

Tensile tests were performed using a uniaxial tensile machine (LSC-50/300, Tokyo Testing Machine, Japan). Dumbbell-shaped specimens with an initial gage length of 10 mm were used for tensile tests. Specimens were cut from the sample films using a dumbbell cutter (SDL-200; Dumbbell, Japan). One of the cross-heads of the uniaxial tensile machine moved at a stretching speed of 10 mm/min; *i.e.,* an initial strain rate of 0.017 s^{-1}. The average value of 10 measurements was calculated for each sample.

Results and discussion

The temperature dependence of dynamic tensile moduli such as the storage

105 modulus (*E'*) and loss modulus (*E"*) for aPLA containing $LiCF_3SO_3$ is shown in Figure
106 1. The profiles in Figure 1 are typical of the dynamic mechanical properties for
107 amorphous polymers. The glassy and transition regions are clearly detected with the
108 end of the rubbery region. The storage modulus in the glassy region is around 2 GPa
109 for pure PLA, which is not affected by the $LiCF_3SO_3$ addition. Around at T_g, the *E'*
110 drops off sharply, whereas the *E"* shows a sharp peak. It is apparent that adding
111 $LiCF_3SO_3$ greatly enhances the T_g. The peak temperature of the *E"*, i.e., the T_g, is
112 located at 65 °C for pure aPLA, 68 °C for aPLA with 10 wt.% $LiCF_3SO_3$, and 72 °C for
113 aPLA with 20 wt.% $LiCF_3SO_3$. The width of the *E"* peak becomes slightly broad, and
114 therefore the *E'* gradually decreases, especially in the high temperature region. This
115 suggests that the relaxation time distribution also becomes broad.

116

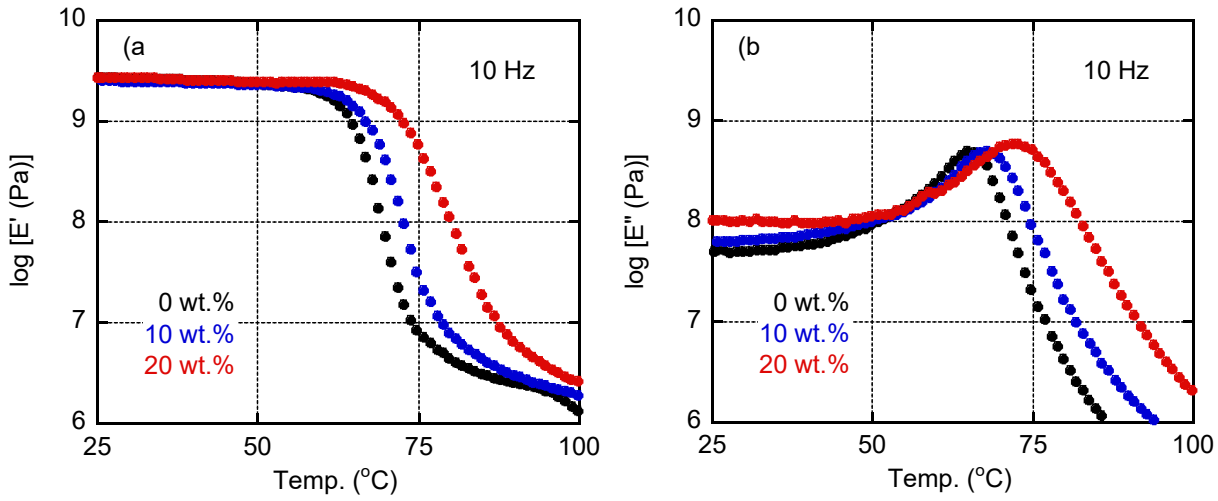

117 **Fig. 1** Temperature dependence of dynamic tensile moduli such as the (a) storage
118 modulus (*E'*) and (b) loss modulus (*E"*) at 10 Hz for (black) aPLA, (blue)
119 aPLA/$LiCF_3SO_3$ (90/10), and (red) aPLA/$LiCF_3SO_3$ (80/20).

120

Photographs of the samples are shown in Figure 2. It is found that adding $LiCF_3SO_3$ improves the heat resistance of aPLA, without loss of optical transparency.

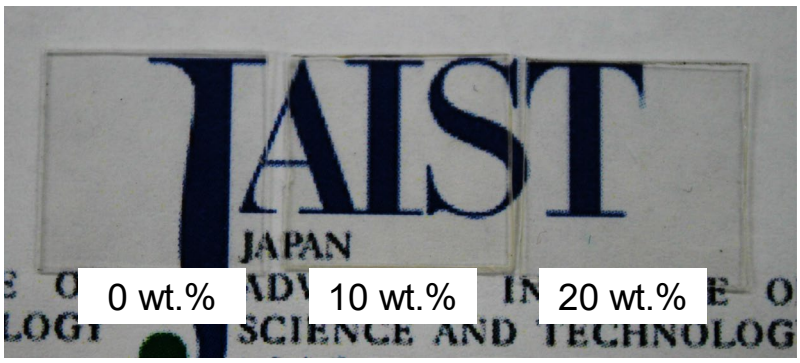

Fig. 2 Photograph of 300-μm-thick films of (left) aPLA, (center) aPLA/$LiCF_3SO_3$ (90/10), and (right) aPLA/$LiCF_3SO_3$ (80/20).

Figure 3 shows the dynamic mechanical properties for cPLA containing $LiCF_3SO_3$. For pure cPLA, the storage modulus significantly decreases at around 60 °C because of the glass-to-rubber transition, and then increases again at above 85 °C. This is attributed to cold-crystallization, which is often observed for crystalline PLA products obtained by rapid cooling [18]. Specifically, the sample preparation conditions employed in this study, i.e., cooling at 25 °C in a compression-molding machine, are quenching conditions which do not allow cPLA to become sufficiently crystallized. Cold-crystallization occurs at high temperatures for the samples containing $LiCF_3SO_3$, because the addition of $LiCF_3SO_3$ enhances the T_g. The modulus finally decreases at 170 °C, which corresponds to the melting point. The melting point decreases with increasing $LiCF_3SO_3$ content. This result suggests that the size of the PLA crystallites generated during the measurement decreases with increasing $LiCF_3SO_3$ content. Cold-

crystallization occurs at high temperature because of the reduced segmental motion, so the crystallites cannot grow as much in samples containing $LiCF_3SO_3$.

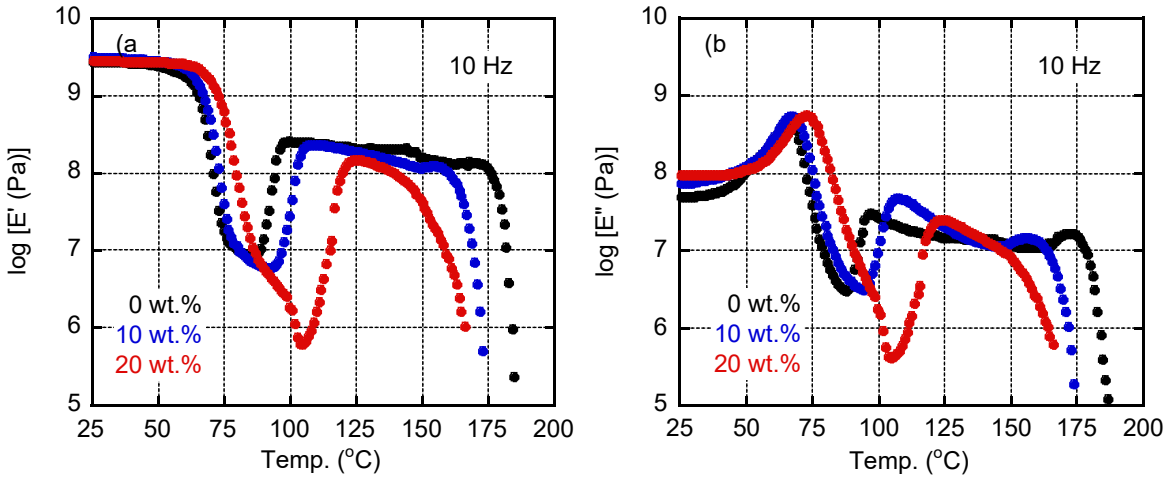

Fig. 3 Temperature dependence of dynamic tensile moduli such as the (a) storage modulus (*E'*) and (b) loss modulus (*E"*) at 10 Hz for (black) cPLA, (blue) cPLA/$LiCF_3SO_3$ (90/10), and (red) cPLA/$LiCF_3SO_3$ (80/20).

The effect of the addition of $LiCF_3SO_3$ on the FT-IR spectra of the blends, particularly on the carbonyl symmetric stretching region, is shown in Figure 4. It is well known that strong electrostatic interaction with oxygen atoms in carbonyl groups provides the shoulder in the low wavenumber region as demonstrated in the blends of PMMA and $LiCF_3SO_3$ [27]. The peak broadens in the low wavenumber region upon the addition of $LiCF_3SO_3$, irrespective of the type of PLA (i.e., aPLA and cPLA). This suggests an ion-dipole interaction between the lithium cations dissociated in PLA and carbonyl groups. This interaction leads to reduced segmental motion, and is responsible for the T_g enhancement and retarded cold-crystallization behavior.

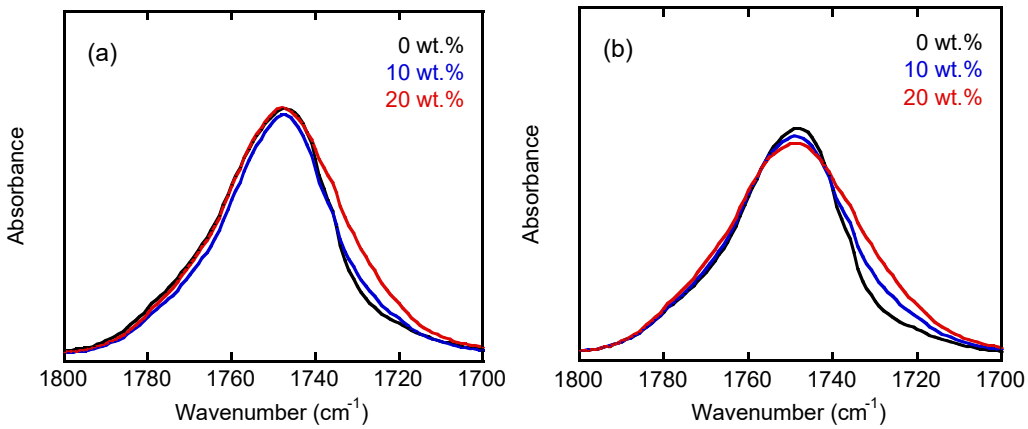

Fig. 4 FT-IR spectra for (a) aPLA/$LiCF_3SO_3$ and (b) cPLA/$LiCF_3SO_3$.

Master curves for the frequency dependence of oscillatory shear moduli are shown in Figure 5. The measurements were performed for the aPLA system, to avoid the effects of crystallization. As seen in the figure, the time-temperature superposition principle is applicable to pure aPLA and aPLA containing $LiCF_3SO_3$, in the temperature range of 90–180 °C.

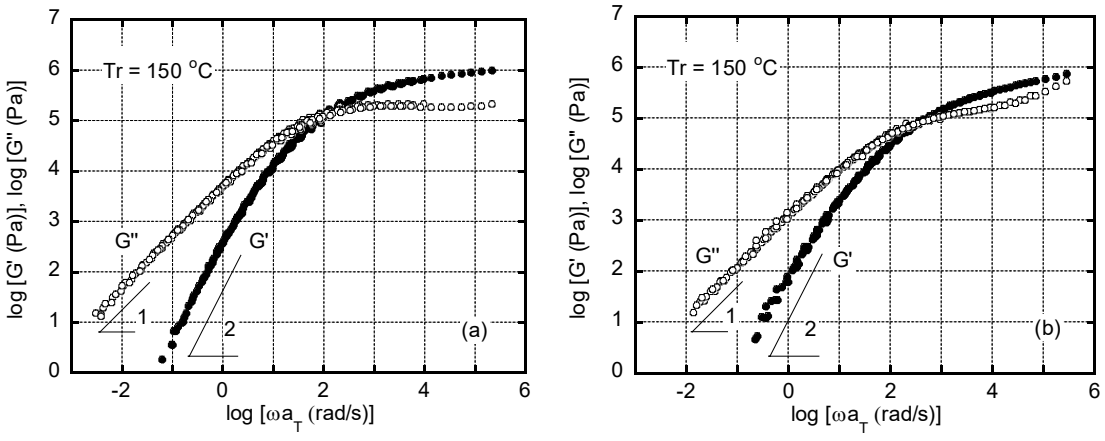

Fig. 5 Master curves of frequency dependence of oscillatory shear moduli at the reference temperature of 150 ºC for (a) aPLA and (b) aPLA/$LiCF_3SO_3$ (80/20).

There is an obvious difference between the samples in the high frequency region. The gap between the storage modulus *G'* and the loss modulus *G"* at high frequencies is large for pure aPLA, indicating that the sample is in a rubbery region even at 10^5 s^{-1}. In contrast, *G"* is almost equal to *G'* at high frequencies (10^5–10^6 s^{-1}) for the aPLA/$LiCF_3SO_3$ (80/20) blend, suggesting the transition region. This is due to the glass-to-rubber transition occurring at high temperature, i.e., at low frequency. The lowest frequency of the rubbery region shifts to high frequency upon the addition of $LiCF_3SO_3$; therefore, the rubbery region of the blend is narrower. In the low frequency region, the flow (terminal) region is clearly detected as reported for conventional PLA samples [33]. Since the slopes of *G'* and *G"* are 2 and 1, respectively, the rheological terminal parameters such as the zero-shear viscosity (η_0), steady-state compliance (J_e^0), and weight-average relaxation time (τ_w), can be calculated from the following equations:

$$\eta_0 = \lim_{\omega \to 0} \frac{G''}{\omega} \quad (1)$$

$$J_e^0 = \lim_{\omega \to 0} \frac{G'}{G''^2} \quad (2)$$

$$\tau_w = \eta_0 J_e^0 \quad (3)$$

The values calculated at the reference temperature 150 °C are $\eta_0 = 5.3\times10^3$ (Pa s), $J_e^0 = 1.4\times10^{-5}$ (Pa^{-1}), and $\tau_w = 7.5\times10^{-2}$ (s) for aPLA, and $\eta_0 = 1.1\times10^3$ (Pa s), $J_e^0 = 6.0\times10^{-5}$ (Pa^{-1}), and $\tau_w = 7.6\times10^{-2}$ (s) for aPLA/$LiCF_3SO_3$ (80/20). The τ_w is almost the same for both samples, although the blend shows a lower η_0. Since the blend shows a higher J_e^0, it has a broad distribution of the relaxation time. The ion-dipole interaction presumably affects the relaxation time distribution.

The ion-dipole interaction also affects the crystallization behavior of cPLA, as indicated in Figure 3. DSC cooling curves for cPLA/$LiCF_3SO_3$ blends at a cooling rate of 2 °C/min are shown in Figure 6. The exothermic peak ascribed to the crystallization is detected at 112 °C for pure cPLA, which is consistent with results from a previous study [10]. The peak shifts to lower temperature upon the addition of 5 wt.% $LiCF_3SO_3$, and becomes very weak in the curve for cPLA/$LiCF_3SO_3$ (90/10). These results demonstrate that adding $LiCF_3SO_3$ retards the crystallization growth for cPLA. This is attributed to the reduced segmental motion of PLA chains by the ion-dipole interaction. Finally, no peak is detected upon the addition of 20 wt.% $LiCF_3SO_3$, despite the slow cooling rate. In other words, 20 wt.% of $LiCF_3SO_3$ is good enough to provide the "anti-crystallization" property for cPLA, leading to a transparent product without scattering entities originated from crystalline structure.

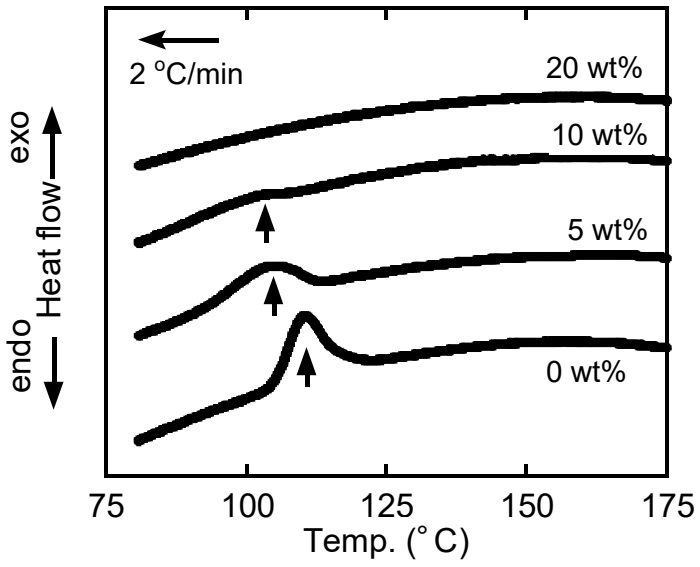

Fig. 6 DSC cooling curves at a cooling rate of 2 °C/min, for cPLA/$LiCF_3SO_3$ with different compositions.

206

207 Furthermore, these results suggest that the blends with $LiCF_3SO_3$ may be utilized
208 for transparent applications with improved heat resistance due to the T_g enhancement
209 even using PLA samples with a low concentration of L-lactide.

210 The mechanical properties in the solid state were evaluated by tensile testing using
211 aPLA/$LiCF_3SO_3$ blends. Stress-strain curves for aPLA/$LiCF_3SO_3$ are shown in Figure
212 7. Both stress and strain are engineering values. As summarized in Table 1, adding
213 $LiCF_3SO_3$ greatly enhances the Young's modulus and yield stress. The results indicate
214 that the rigidity is effectively enhanced by the ion-dipole interaction. In contrast, the
215 blends exhibit brittle behavior, which leads to the decrease in the mechanical toughness.
216 This problem will be severe as increasing the $LiCF_3SO_3$ content. Presumably, the
217 applied stress of the blends is beyond the critical one of crazing, or the critical stress
218 for shear yielding increases upon the addition of $LiCF_3SO_3$. Moreover, the decrease in
219 the density of the entanglement couplings by the $LiCF_3SO_3$ addition, which is believed
220 to provide brittle fracture, plays an important role. In either mechanism, another
221 technique will be required to improve the mechanical toughness of the blends with
222 $LiCF_3SO_3$. The addition of rubbery materials, one of the most well-known methods,
223 and the appropriate annealing treatment to reduce the critical stress for shear yielding,
224 which leads to ductile behavior as reported recently [30,31], are highly recommended.

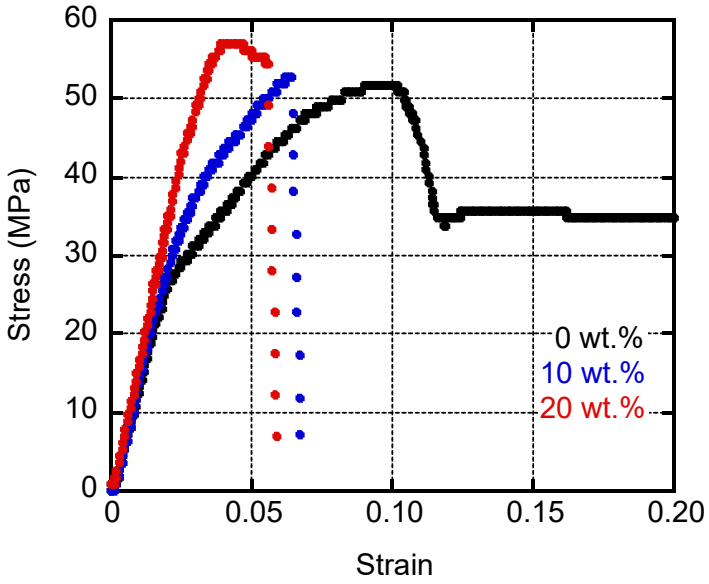

225

226 **Fig. 7** Stress-strain curves for aPLA/$LiCF_3SO_3$ with different compositions.

227

228 Table 1 Tensile properties of aPLA/$LiCF_3SO_3$ blends

$LiCF_3SO_3$ content (wt.%)	Young's Modulus (GPa)	Yield Stress (MPa)	Elongation at Break (%)
0	1.50	51.7	340
10	1.68	52.8	6
20	1.79	57.1	6

229

230 **Conclusion**

231 The structures and properties of PLA/$LiCF_3SO_3$ blends were studied. Adding
232 $LiCF_3SO_3$ restricts the segmental motion of the PLA chains. This is attributed to the
233 ion-dipole interaction, which is pronounced at around the T_g. As a result, the T_g is
234 enhanced for both aPLA and cPLA, without loss of transparency. The Young's modulus
235 and yield stress of aPLA are also enhanced by adding $LiCF_3SO_3$ with the reduced
236 mechanical toughness due to brittle fracture. The restricted segmental motion greatly
237 decreases the crystallization rate. Consequently, the crystallization peak is not detected

for cPLA/$LiCF_3SO_3$ (80/20), even at a slow cooling rate of 2 °C/min. Cold-crystallization, which is detected by dynamic mechanical analysis, occurs at higher temperature upon the addition of $LiCF_3SO_3$ because of the T_g enhancement with the restricted segmental motion. The ion-dipole interaction becomes weak at high temperature. Therefore, the rheological terminal region is clearly detected. This suggests that adding $LiCF_3SO_3$ does not significantly affect the melt-processability, although it broadens the distribution of the terminal relaxation mode. Considering that the ion-dipole interaction between the carbonyl group and lithium cation is responsible for the phenomenon, a similar result is expected for various polyester materials.

ACKNOWLEDGEMENTS

A part of this work was supported by JSPS Grant-in-Aid for Scientific Research (B) Grant Number 16H04201.

Reference

[1] Auras R, Lim LT, Selke SEM, Tsuji H (2010) Poly(lactic acid): synthesis, structures, properties, processing, and applications, Wiley, Hoboken.

[2] Saeidlou S, Huneault MA, Li H, Park CB (2012) Poly(lactic acid) crystallization. Prog Polym Sci 37:1657-1677.

[3] Jimenez J, Peltzer M, Ruseckaite R (2014) Poly(lactic Acid) science and technology: Processing, properties, additives, and applications. Royal Society of Chemistry, Oxfordshire.

[4] Yamaguchi M (2016) Manufacturing of high performance biomass-based polyesters by rheological approach. in: V.K. Thakur, M.K. Thakur (Eds.), Handbook of composite from renewable materials. Wiley, New York, Chap. 2.

[5] Lorenzo MRD, Androsch R (2018) Synthesis, structure and properties of poly(lactic

264 acid). Springer.
265 [6] Dubey SP, Thakur VK, Krishnaswamy S, Abhyankar HA, Marchante V, Brighton
266 JL (2017) Progress in environmental-friendly polymer nanocomposite material
267 from PLA: Synthesis, processing and applications. Vacuum 146:655-663.
268 [7] Krepsztul JW, Rydzkowski T, Borowski G, Szczypinski M, Klepka T, Thakur VK
269 (2018) Recent progress in biodegradable polymers and nanocomposite-based
270 packaging materials for sustainable environment. Int J Polym Anal Charact 23:383-
271 395.
272 [8] Madhumitha G, Fowsiya J, Roopan SM, Thakur VK (2018) Recent advances in
273 starch–clay nanocomposites. Int J Polym Anal Charact 23:331-345.
274 [9] Dorgan J, Lehermeir H, Mang M (2000) Thermal and rheological properties of
275 commercial grade poly(lactic acid)s. J Polym Environ 8:1-9.
276 [10] Huang T, Miura M, Nobukawa S, Yamaguchi M (2014) Crystallization behavior
277 and dynamic mechanical properties of poly(L-lactic acid) with poly(ethylene
278 glycol) terminated by benzoate. J Polym Environment 22:183-189.
279 [11] Ray SS, Okamoto M (2003) Polymer/layered silicate nanocomposites: a review
280 from preparation to processing. Prog Polym Sci 28:1539-1641.
281 [12] Nam JY, Okamoto M, Okamoto H, Nakano M, Usuki A, Matsuda M (2006)
282 Morphology and crystallization kinetics in a mixture of low-molecular weight
283 aliphatic amide and polylactide. Polymer 47:1340-1347.
284 [13] Liao R, Yang B, Yu W, Zou C (2007) Isothermal cold crystallization kinetics of
285 polylactide/nucleating agents. J Appl Polym Sci 104:310-317.
286 [14] Wu J, Zou X, Jing B, Dai W (2015) Effect of sepiolite on the crystallization
287 behavior of biodegradable poly(lactic acid) as an efficient nucleating agent.
288 Polym Eng Sci 55:1104-1112.
289 [15] Zou GX, Jiao QW, Zhang X, Zhao CX, Li JC (2015) Crystallization behavior and
290 morphology of poly(lactic acid) with a novel nucleating agent. J Appl Polym Sci
291 132:41367.
292 [16] Sheth M, Kumar RA, Dave V, Gross RA, MaCarthy SP (1997) Biodegradable
293 polymer blends of poly(lactic acid) and poly(ethylene glycol). J Appl Polym Sci

66:1495-1505.2009

[17] Okamoto K, Ichikawa T, Yokohara T, Yamaguchi M (2009) Miscibility, Mechanical and Thermal Properties of Poly(lactic acid)/polyester-diol blends. Eur Polym J 45:2304-2312.

[18] Hassouna F, Raquez JM, Addiego F, Dubois P, Toniazzo V, Ruch D (2011) Grafting of poly (ethylene glycol) (PEG) via reactive extrusion. Eur Polym J 47:2134-2144.

[19] Gedde UW (1995) Polymer Physics, Kluwer Academic Publishers, Dordrecht.

[20] Bicerano J (2011) Glass transition, in: J. Bailey (Ed.) Properties and behavior of polymers, Wiley, Hoboken.

[21] Mitomo M, Kaneda A, Quynh TM, Nagasawa N, Yoshii F (2005) Improvement of heat stability of poly(L-lactic acid) by radiation-induced crosslinking. Polymer 46:4695-4703.

[22] Yang LS, Wu HZ, Yang W, Yang BM (2008) Thermal and mechanical properties of chemical crosslinked polylactide (PLA). Polym Test 27:957-963.

[23] Rahmat M, Ghasemi I, Karrabi M, Azizi H, Zandi M, Riahinezhad M (2015) Silane crosslinking of poly(lactic acid): The effect of simultaneous hydrolytic degradation. eXPRESS Polym Lett 9:1133-1141.

[24] Eisenberg A, Kim JS (1998) Introduction to ionomers, Wiley, New York.

[25] Vanhoorne P, Jerome R, Teyssie P, Laupretre F (1994) Direct NMR evidence for a local restriction in the segmental chain mobility of a model ionomer. Macromololecules 27:2548-2552.

[26] Ro JA, Huang JS, Weiss AR (2008) Synthesis and thermal properties of telechelic poly(lactic acid) ionomers. Polymer 49:422-431.

[27] Miyagawa A, Ayerdurai V, Nobukawa S, Yamaguchi M (2016) Viscoelastic properties of poly(methyl methacrylate) with high glass transition temperature by lithium salt addition. J Polym Sci Polym Phys Ed 54:2388-2394.

[28] Ito A, Phulkerd P, Ayerdurai V, Soga M, Courtoux A, Miyagawa A, Yamaguchi M (2018) Effects of residual solvent on glass transition temperature of poly(methyl methacrylate). Polym J in press. DOI: 10.1038/s41428-018-0080-4.

[29] Tsugawa N, Ito A, Yamaguchi M (2018) Effect of lithium salt addition on the

structure and optical properties of PMMA/PVB blends. Polymer 146:242-248.

[30] Huang T, Miura M, Nobukawa S, Yamaguchi M (2015) Chain packing and its anomalous effect on mechanical toughness for poly(lactic acid). Biomacromol. 16:1660-1666.

[31] Huang T, Yamaguchi M (2017) Effect of cooling conditions on the mechanical properties of crystalline poly(lactic acid). J Appl Polym Sci 134:44960.

[32] Ito A, Ayerdurai V, Miyagawa A, Matsumoto A, Okada H, Courtoux A, Yamaguchi M (2018) Effects of residual solvent on glass transition temperature of poly(methyl methacrylate). Nihon Reoroji Gakkaishi 46:117-121.

[33] Yokohara T, Yamaguchi M (2008) Structure and properties for biomass-based polyester blends of PLA and PBS. Eur Polym J 44:677-685.